On the importance of chain branching in tear film lipid layer wax and cholesteryl esters

Viitaja, Tuomo

2022-06

Viitaja , T , Raitanen , J-E , Hynynen , A , Moilanen , J , Svedström , K , Paananen , R O & Ekholm , F S 2022 , ' On the importance of chain branching in tear film lipid layer wax and cholesteryl esters ' , Colloids and Surfaces B: Biointerfaces , vol. 214 , 112429 . https://doi.org/10.1016/j.colsurfb.202

http://hdl.handle.net/10138/344222
https://doi.org/10.1016/j.colsurfb.2022.112429

Colloids and Surfaces B: Biointerfaces 214 (2022) 112429

Contents lists available at ScienceDirect

Colloids and Surfaces B: Biointerfaces

journal homepage: www.elsevier.com/locate/colsurfb

On the importance of chain branching in tear film lipid layer wax and cholesteryl esters

Tuomo Viitaja [a,b,1], Jan-Erik Raitanen [a,1], Antti Hynynen [a], Jukka Moilanen [b], Kirsi Svedström [c], Riku O. Paananen [a,b,*], Filip S. Ekholm [a,**]

[a] Department of Chemistry, University of Helsinki, P.O. Box 55, Helsinki FI-00014, Finland
[b] Ophthalmology, University of Helsinki and Helsinki University Hospital, Haartmaninkatu 8, Helsinki FI-00290, Finland
[c] Department of Physics, University of Helsinki, P.O. Box 64, Helsinki FI-00014, Finland

ARTICLE INFO

Keywords:
Biophysics
Chemical synthesis
Structural elucidation
Tear film lipid layer

ABSTRACT

The tear film lipid layer (TFLL) is important to the maintenance of ocular surface health. Surprisingly, information on the individual roles of the myriad of unique lipids found therein is limited. The most abundant lipid species are the wax esters (WE) and cholesteryl esters (CE), and, especially their branched analogs. The isolation of these lipid species from the TFLL has proved to be tedious, and as a result, insights on their biophysical profiles and role in the TFLL is currently lacking. Herein, we circumvent these issues by a total synthesis of the most abundant *iso*-methyl branched WEs and CEs found in the TFLL. Through a detailed characterization of the biophysical properties, by the use of Langmuir monolayer and wide-angle X-ray scattering techniques, we demonstrate that chain branching alters the behavior of these lipid species on multiple levels. Taken together, our results fill an important knowledge gap concerning the structure and function of the TFLL on the whole.

1. Introduction

The tear film lipid layer (TFLL) that covers the ocular surface is a unique biological membrane that forms the outermost layer of the tear film. It stabilizes the tear film, and plays a crucial role in the maintenance of ocular surface health. The TFLL is secreted by the Meibomian glands and has a highly conserved and specific composition encompassing a number of lipid classes such as wax esters (WEs), cholesteryl esters (CEs), *O*-acyl-ω-hydroxy fatty acids (OAHFAs), type I-St and type II diesters, triglycerides, and free cholesterol [1–5]. Herein we will focus on the WEs and CEs which are the most abundant lipid classes in the TFLL. In fact, these species constitute roughly 75–95% of the entire TFLL lipidome [1–5]. In the past, the majority of studies on TFLL WEs and CEs have been performed with straight-chain lipid species or simplified structural analogs [6–21]. This is surprising as the majority of these TFLL lipids actually exist in their *iso* or *anteiso*-branched forms [1,22,23]. A pioneering study by Nicolaides et al. showed that roughly 75% of the CEs, and, 70% of the WEs are branched [1], and additional confirmation on the extensive nature of branching has been supplied by NMR spectroscopic techniques [24,25]. While so, the isolation of branched CEs and WEs in sufficient quantities and purities from the TFLL has proved to be a difficult task that is further complicated by the large number of lipid species present, the minute amounts of meibum available, and the inter-individual variations in TFLL composition. Due to the unavailability of these lipid species, the effects of branching on the biophysical profiles of TFLL CEs and WEs remains unclear, and as a result, the correlation to proper TFLL function is unknown.

In light of the existing literature information on other lipid species [26–30], *iso*- and *anteiso* methyl branching has a fluidizing effect on the hydrocarbon chains, and lowers the melting points of the lipids. Therefore, it seems plausible that methyl branching could alter the type of ordered structures formed by Meibomian lipids in the TFLL and affect its function. In order to explore the effects of methyl branching on the biophysical properties of TFLL CEs and WEs, we set out to synthesize and study the biophysical profiles of the most abundant *iso*-methyl branched CEs and WEs (see Fig. 1 for an overview of our study design). In addition, the corresponding straight-chain analogs were synthesized in order to allow direct comparison of the biophysical profiles. Our study shows

* Corresponding author at: Department of Chemistry, University of Helsinki, P.O. Box 55, Helsinki FI-00014, Finland.
** Corresponding author.
E-mail addresses: riku.o.paananen@helsinki.fi (R.O. Paananen), filip.ekholm@helsinki.fi (F.S. Ekholm).
[1] Equal contribution.

https://doi.org/10.1016/j.colsurfb.2022.112429
Received 4 January 2022; Received in revised form 22 February 2022; Accepted 23 February 2022
Available online 25 February 2022

that *iso*-methyl branching has a considerable effect on the biophysical properties and function of the TFLL lipids.

2. Materials and methods

All reagents were purchased from commercial sources unless otherwise stated. Dry solvents were purified by the VAC vacuum solvent purification system prior to use when required. All reactions containing moisture- or air-sensitive reagents were carried out under an argon atmosphere. Reactions requiring heating were performed in an external oil bath equipped with a heat sensor and temperature controller. Flash chromatography was carried out on silica gel 40. TLCs (Thin-layer chromatography) were performed on aluminum sheets pre-coated with silica gel 60 F254 (Merck). Spots were visualized by spraying with an 1:4 H_2SO_4/MeOH-solution or staining with Phosphomolybdic acid (10%, w/v in EtOH) followed by charring. HRMS (High-resolution Mass Spectrometry) were recorded with a Bruker Micro Q-TOF instrument featuring ESI (electrospray ionization) in positive mode. NMR spectra were recorded with a Bruker Avance III NMR spectrometer operating at 499.82 MHz (^{1}H) and 125.68 MHz (^{13}C). The probe temperature was kept at 25 °C unless otherwise stated. A number of 1D (^{1}H and ^{13}C) and 2D experiments (DQF-COSY (Double Quantum Filtered COrrelation SpectroscopY), TOCSY (TOtal Correlation SpectroscopY), Ed-HSQC (Edited Heteronuclear Single Quantum Coherence), HSQC-TOCSY, HMBC (Heteronuclear Multiple Bond Correlation) and ROESY (Rotating frame Overhauser Effect SpectroscopY) were recorded with pulse sequences provided by the instrument manufacturer. The spectra were processed in Bruker Topspin 4.0.7 software and the chemical shifts and coupling constants in the ^{1}H NMR spectra were further analyzed by quantum mechanical modeling using the PERCH (PEak reseaRCH) NMR software [31]. In the reported data, the chemical shifts are expressed on the δ scale (in ppm) using TMS (tetramethylsilane), residual chloroform, or chloroform/methanol as an internal standard. The coupling constants are given in Hz (Hertz) and provided only once when first encountered whereas the coupling patterns are given as s (singlet), d (doublet), t (triplet) or m (multiplet) etc. Melting point analysis was performed using a Büchi B-545 melting point instrument (BÜCHI Labortechnik AG, Flawil, Switzerland), or, a Mettler Toledo MP50 (Columbus, OH, USA) melting point system when found relevant.

The Langmuir trough experiments were conducted with a KSV NIMA Langmuir large trough (Biolin Scientific, Espoo, Finland; dimensions 580 × 145 mm) filled with a PBS (Phosphate-buffered saline) buffer. Lipids were administered at the air-buffer interface in a chloroform solution with a concentration of 6.46 mM (*n*-WE), 8.07 mM (*iso*-WE), 3.45 mM (*n*-CE) and 5.36 mM (*iso*-CE). Previous studies have shown that the ambient ozone readily oxides unsaturated wax esters [32]. To prevent oxidation, the measurement setup was contained in an acrylic enclosure (volume 290 L), and dry air was continuously passed through an ozone solutions ODS-3 P ozone destruct unit (Hull, Iowa) and into the enclosure at a rate of 76 L/min to maintain a low-ozone atmosphere. During the compression, surface pressure was measured using a Wilhelmy plate and the surface potential was measured using KSV SPOT (Espoo, Finland). BAM (Brewster Angle Microscopy) images were captured using a KSV NIMA microBAM camera (Espoo, Finland). A circulating water bath (LAUDA ECO E4) was used to control the temperature of the subphase. Measurements were performed at 33 ± 1, 35 ± 1, and 40 ± 1 °C for all lipids. The evaporation resistance of lipid films were determined using a modified Langmuir-Schaefer method [33], for more details see our previous work [16,34,35]. The Langmuir trough measurements were repeated at least four times.

The crystalline structures of the WE and CE bulk samples were studied using WAXS both at room temperature and at physiological temperature (34 °C). In addition to the synthesized lipids, standard samples of arachidyl oleate, behenyl oleate, cholesteryl stearate, and cholesteryl behenate obtained from Nu-Check Prep (Elysian, MN, USA) were measured for comparison. The WAXS measurements were carried out in perpendicular transmission geometry using a copper anode X-ray tube (Malvern Panalytical, Malvern, UK) and a generator (Seifert) (25 mA, 36 kV). The beam was monochromated by a Montel monochromator (Incoatec GmbH, Geesthacht, Germany) selecting the Cu Kα wavelength (λ = 1.541 Å). The length of the scattering vector (q) was 0.15–3.3 1/Å and it was calibrated using lanthanum hexaboride (LaB_6). The scattering patterns were collected by a MAR345 image plate (Marresearch GmbH, Norderstedt, Germany). Each sample was measured between mylar foils in a washer for 30 min at both temperatures. The data was integrated from 80° sector, and geometrical and polarization corrections were applied, in addition to absorption correction and background correction due to scattering arising from both the air and mylar backgrounds. After the sample was measured at room temperature, it was heated in situ using a Linkam heating stage with a gradient of 10 °C/min. The temperature was let to stabilize for 10 min and then the scattering pattern was collected for 30 min. The temperature was determined to be 34 ± 1 °C at the surface of the washer. The d spacing was obtained based on the position of the diffraction peak *hkl* as: $d_{hkl} = 2\pi/q_{hkl}$.

3. Results and discussion

3.1. Total synthesis and structural characterization of a naturally occurring iso-methyl branched CE and WE

In the TFLL, WEs and CEs exist as straight-, *iso*-branched and *anteiso*-

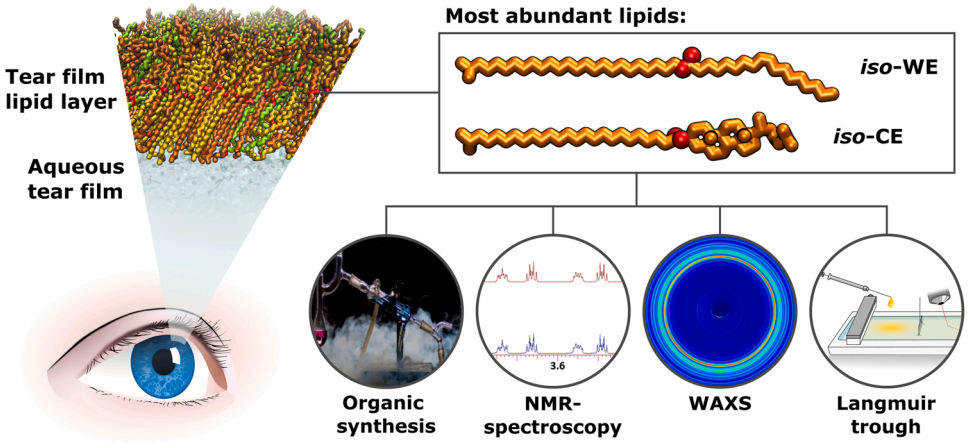

Fig. 1. Overview of the study design, including the studied *iso*-branched lipids (*iso*-WE and *iso*-CE) and key experimental techniques utilized. NMR: Nuclear Magnetic Resonance; WAXS: Wide Angle X-ray Scattering.

branched isomers with chain lengths varying from 38 to 50 carbon atoms when the entire backbone is accounted for [1,2,4,5,36–38]. While the diversity is rich, the most abundant of these lipids are the ones which feature a 25-carbon long *iso*-methyl branched carboxylic acid coupled to cholesterol (in the case of CEs), and, a WE composed from oleic acid and the corresponding 25-carbon long *iso*-methyl branched alcohol. These two species make up roughly 10–14% of the total CEs, and, 13–20% of the total WEs in the TFLL [1]. Surprisingly, reports on the total synthesis of these and other long-chain *iso*-branched WEs and CEs found in the TFLL are scarce in the literature. Access to these species in their pure form is crucial to mapping their role in the TFLL and generating an increased understanding of this unique biological membrane. Thus, we selected these representative lipids as our primary synthetic targets and performed a retrosynthetic analysis in order to plan their synthetic routes. The retrosynthetic analysis is displayed in Fig. 2.

In short, the synthesis of both the *iso*-methyl branched WE and CE can be achieved through a shared intermediate starting from fragments A and B. Fragment A can be prepared from 1,20-eicosanedioic acid in three steps according to literature protocols [39], and fragment B is commercially available. Thus, the starting point is ideal. The choice of protective groups, leaving groups, and conjugation protocols were based on both the experience gained through our recent work on the synthesis of other TFLL-lipids such as *O*-acyl-ω-hydroxy fatty acids, and, type I-St/type II diesters [35], as well as a careful examination of the protocols employed by other research groups active in the field [39,40]. The main differences to our earlier work is that we chose to employ a THP-protective group in fragment A in order to avoid the shortcomings caused by the silyl ether previously, and, we opted to explore an alkynylation-reduction coupling sequence in order to improve upon the dissatisfying yields obtained through a Wittig reaction [35]. It should be noted that while we in the synthesis discussion below focus on the most abundant *iso*-methyl branched TFLL WE and CE species, we did synthesize their corresponding straight-chain analogs in order to study, verify and validate the effect of branching. Details on the synthesis of the straight-chain analogs are reported in the Supporting Information. Overall, the appeal of the general synthetic strategy highlighted above is that it can be employed in the preparation of a large amount of naturally occurring TFLL lipids, and structural analogs thereof (with variations in chain length, branching patterns, functional groups etc.).

The synthetic routes to *iso*-WE (**4**) and *iso*-CE (**6**) are displayed in Scheme 1. While discussing the synthesis, we will simultaneously address the validation protocols utilized to ascertain the molecular structures of the products at key steps. We consider this to be of upmost importance, and have noticed that the literature data on TFLL-lipids is in part inadequate in this regard. Here we will especially highlight the information obtained with appropriate NMR-spectroscopic techniques (the complete characterization data is supplied in the Supporting Information).

Our work started with the synthesis of Fragment A (**1**) from 1,20-eicosanedioic acid. Despite the fact that both the reduction with lithium aluminum hydride (LAH) and the monobromination protocol have been reported frequently in the literature [41–44], these reactions are challenging to perform on long-chain lipid species due to the limited solubility of the intermediate diol. For example, continuous and thorough washing was required during the work-up step of the reduction in order to obtain 1,20-eicosanediol in an 87% yield, and, the monobromination yield was significantly lower than that obtained previously with shorter diols such as 1,12-dodecanediol (52% vs. 77%) [34]. Upon monobromination, the solubility changed drastically and the THP-ether could be introduced without difficulties in a 96% yield following the protocol of Beck et al. [45] Despite being a widely employed protecting group, the NMR signals of the THP group are not routinely fully assigned with NMR [46,47]. In principle, the THP ether can exist as a mixture of stereoisomers and in several different conformations, however, in our case, the coupling patterns observed in the ^{1}H NMR spectra suggested that this was not the case. Here, we used 2D NMR-spectroscopic techniques to assign the ^{1}H and ^{13}C signals of the THP group (and entire molecule) and quantum mechanical modeling in order to analyze the key coupling constants. We arrived at the conclusion that the $^{4}C_{1}$-chair is the dominating conformation, and that the C-2′-substituent occupies an axial position. This was deduced based on the following coupling constants: $J_{2',3'a} = 2.8$ Hz, $J_{2',3'b} = 4.6$ Hz for H-2′; $J_{6'a,5'b} = 3.0$ Hz, $J_{6'a,5'a} = 8.1$ Hz, $J_{6'a,6'b} = -11.1$ Hz for H-6′a; $J_{4'a,3'b} = 3.6$ Hz, $J_{4'a,5'a} = 7.9$ Hz, $J_{4'a,3'a} = 9.3$ Hz, $J_{4'a,4'b} = -12.0$ Hz for H-4′a. In more detail, the coupling constants for H-2′ are indicative of equatorial-equatorial and equatorial-axial coupling patterns thus suggesting that H-2′ occupies an equatorial position. The large and small coupling constants observed for the other signals spread throughout this moiety follow the trends typically observed in carbohydrate ^{1}H NMR spectra (D-glucose, D-mannose, D-galactose etc.) [48–50] and are indicative of a $^{4}C_{1}$-chair conformation (axial-axial coupling constants ~ 9 Hz, equatorial-axial coupling constants ~ 4 Hz; and geminal coupling constants ~ −12 Hz). While we did not notice the formation of stereoisomers, the THP-ether induced diastereotopicity in the H-1 protons, which as a result split into two separate signals at 3.73 ppm and 3.38 ppm, respectively. With the questions surrounding the THP-ether resolved, and access to both **1** (Fragment A) and Fragment B (4-methyl-1-pentyne) secured, we proceeded with the alkynylation protocol.

The slightly acidic terminal alkyne was successfully deprotonated in situ with BuLi, and the resulting nucleophile was coupled with **1** in a S_N2-type fashion with the bromide serving as a leaving group. The isolated yield of **2** was excellent (89%) which is indicative of a strategy superior to our previously utilized Wittig protocol [35]. Nevertheless, a few observations should be further highlighted. First, the reaction did not proceed efficiently in the absence of HMPA thus indicating that a co-solvent capable of solvating cations is beneficial to the formation of acetylide anions. In addition, the reaction conditions were tailored for the purpose; an excess of the cheap alkyne was utilized, TBAI was added in order to increase the reactivity of **1** through displacement of the bromide with iodide, and the conjugation reaction was performed at elevated temperatures. The ^{1}H and ^{13}C NMR spectra of **2** were solved and the majority of the chemical shifts and coupling constants were similar to those observed in the individual fragments A and B, with the exception of the newly generated chain-elongated alkyne, which well-resolved signals nevertheless appeared at the typical chemical shifts in the spectra. An excerpt of the NMR-spectroscopic characterization is provided in Fig. 3 and the bottom panel showcases the accuracy of the simulated ^{1}H NMR spectra vs. the measured one using **2** as the model substrate.

A mild hydrolysis of the THP-ether was performed with a catalytic

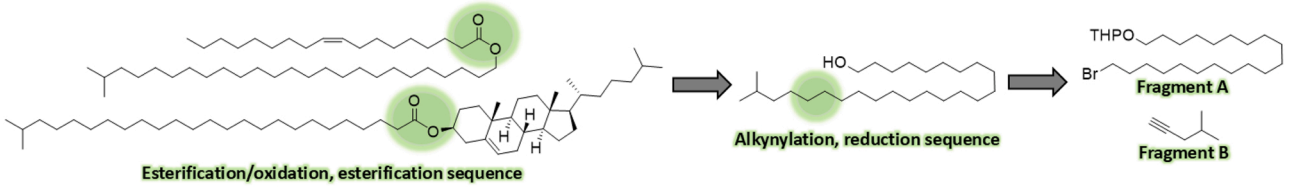

Fig. 2. The retrosynthetic analysis revealed that the most abundant TFLL CE and WE can be constructed from two starting fragments (denoted A and B) through a shared reaction intermediate.

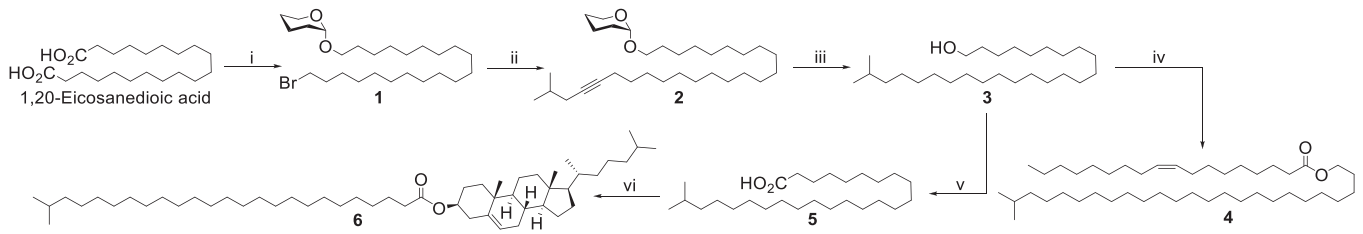

Scheme 1. Overview of the reaction routes and isolated yields: i) 1) $LiAlH_4$, dry THF, reflux, 18 h, 87%; 2) 48% aq. HBr, cyclohexane, reflux, 5 h, 52%; 3) DHP, PPTS, dry CH_2Cl_2, o/n, 96%; ii) 1) 4-methyl-1-pentyne, *n*-BuLi, −78 °C → −40 °C, 2 h; 2) **1**, −78 °C, rt, TBAI, 10 min; then reflux o/n, 89%; iii) 1) CSA, THF:MeOH (1:3), rt, o/n, 95%; 2) Pd/C (10%), dry EtOAc, H_2 (6 bar), 4 h, 83%; iv) Oleic acid, DMAP, EDC·HCl, CH_2Cl_2, rt, o/n, 96%; v) Jones reagent, THF:Acetone:EtOAc (2:2:1), rt, 90 min, 95%; vi) Cholesterol, $NaHSO_4{\cdot}H_2O$ (20 mol-%), 4 mbar, 150 °C, 4 h, 66%.

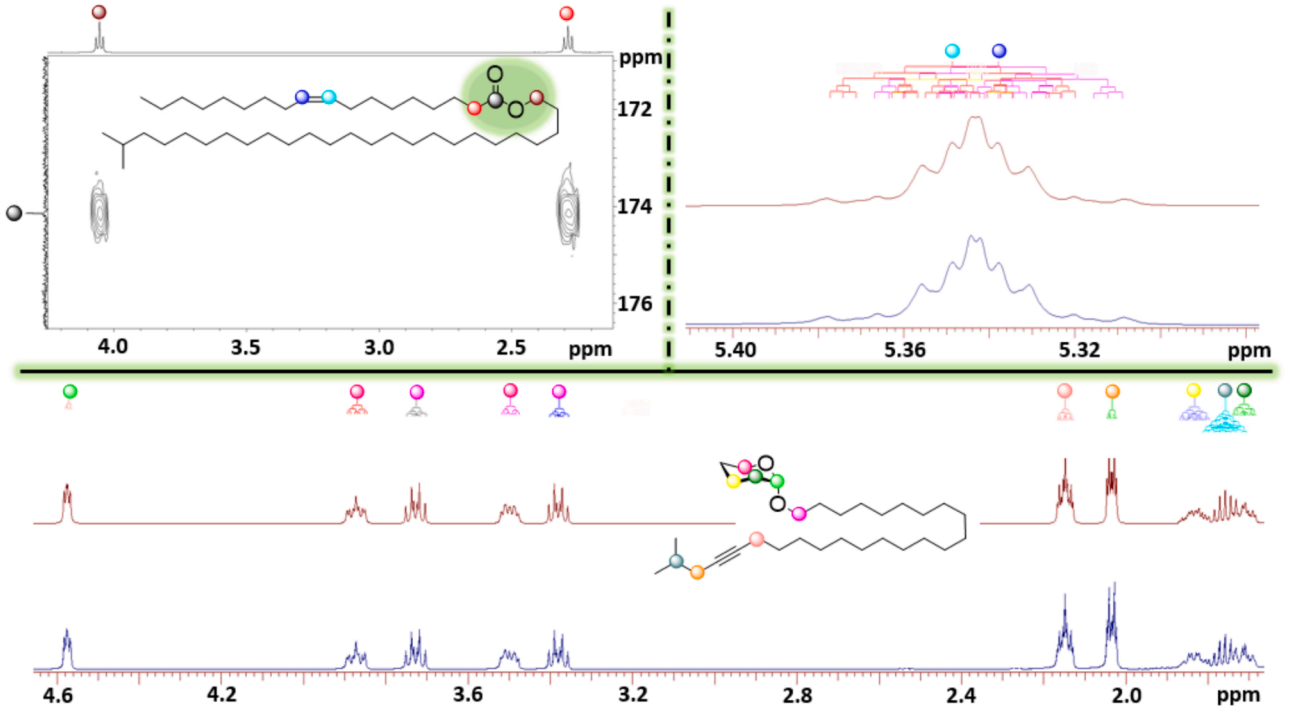

Fig. 3. An excerpt of the NMR spectroscopic characterization studies. The top panel highlights information used to ascertain the structure of **4**. **Top left:** The HMBC cross peaks confirm the location of the ester bond. **Top right:** The 5.41 − 5.28 ppm region of the ^{1}H NMR spectrum of **4** highlights the determination of the (*Z*)-configuration by the use of coupling constants acquired through spectral simulations with PERCH (bottom: measured spectrum, top: simulated spectrum). **Bottom panel**: The 4.60–1.75 ppm region of the ^{1}H NMR spectrum of **2** highlights the accuracy of the spectral simulations with the PERCH software on a general level (bottom: measured spectrum, top: simulated spectrum).

amount of CSA and the triple bond was reduced in a subsequent catalytic hydrogenation reaction employing Pd/C as the catalyst. Through this two-step protocol, the crucial *iso*-methyl branched intermediate **3** could be isolated in a 79% overall yield. A Steglich-type esterification of **3** with commercially available oleic acid gave the most abundant TFLL WE, i.e. **4**, in a 96% yield. In the literature, the chemical structures of the majority of TFLL WEs, and other lipid species present, have been identified through the use of mass spectrometry-based techniques [38,39,51,52]. While such techniques are often a necessity due to the minute amounts of TFLL samples available, we consider that alternative NMR spectroscopic techniques offer significant advantages when sample availability is not a limiting factor. Hence, instead of determining the location of the ester-moiety indirectly through studying fragmentation patterns, we used the HMBC experiment. As showcased in Fig. 3, HMBC cross peaks were observed between the carbonyl carbon (C-1′ at 174.1 ppm) and both H-1 (at 4.05 ppm), and, H-2′ (at 2.29 ppm) thus confirming the location of the ester group. Moreover, we used quantum mechanical simulations employing the PERCH software to solve the complex coupling patterns of the double bond (5.35–5.34 ppm region) in the oleate in order to ascertain that the (*Z*)-configuration remained intact during the reaction and purification step since this is the configuration which the naturally occurring TFLL lipids exist in. The 11.1 Hz coupling constant observed between H-9′–H-10′ is characteristic of the (*Z*)-configuration and in agreement with literature values often cited [53]. Thus, the synthesis of the *iso*-methyl branched TFLL WE was successful.

In order to synthesize *iso*-CE **6**, the intermediate *iso*-methyl branched alcohol **3** was converted to *iso*-cerotic acid (**5**) through our standard Jones oxidation protocol. The solubility issues encountered in this step were circumvented by careful selection of the reaction solvent (THF: Acetone:EtOAc, 2:2:1), and, the isolated yield was 95%. While this yield is in the typical range observed for Jones oxidation protocols [40,54,55], it should be noted that early attempts at the synthesis of **5** through e.g. electrolysis reactions have not been equally successful (yields around 10% reported) [56]. With access to **5** secured, only an esterification reaction with cholesterol remained. We initially evaluated the esterification protocol successfully employed in the synthesis of WE **4** but found it lacking in this case (isolated yields ~ 20%). Therefore, we opted to

perform the reaction under neat conditions (at 150 °C under vacuum) employing sodium bisulfate as the catalyst. We have used this protocol in the past [34], although in this particular case, the temperature was raised slightly in order to reach a liquid reaction state. While the reaction conditions were not fully optimized, the most abundant TFLL CE **6** could through this reaction be isolated in a decent 66% yield. In order to verify the structure of *iso*-CE **6**, we used a similar set of NMR spectroscopic techniques as described above. While we were able to identify all of the signals in the complex ^{1}H and ^{13}C NMR spectra, we were not able to deduce the coupling constants for individual signals in areas with severe overlap.

To summarize, the two most abundant TFLL CEs and WEs, i.e. the *iso*-methyl branched WE (**4**, *iso*-WE) and CE (**6**, *iso*-CE) were prepared in seven and nine synthetic steps with overall yields of 29% (**4**), and, 19% (**6**), respectively. While not discussed above, the corresponding naturally occurring straight-chain analogs were likewise prepared (*n*-WE; *n*-CE, see the Supporting Information). During the completion of the synthetic routes, all of the products, and intermediates, were purified by state-of-the-art techniques and characterized in detail by NMR-spectroscopy (1D and 2D techniques), further coupled with quantum mechanical spectral simulations with the PERCH software, and HRMS. The purity of the four lipid species evaluated in the biophysical studies exceeded 95% (see NMR spectra in the Supporting Information).

3.2. *Iso-methyl branching alters the melting points and bulk crystal structures of WEs and CEs*

It has been estimated that branching of tear film lipids likely lowers the melting point of meibum by 20−40 °C, i.e. to near body temperature, which is likely essential for spreading of meibum onto the ocular surface [23]. To evaluate this hypothesis, the first step was to determine and compare the melting points of the synthesized *iso*-branched and straight-chain CEs and WEs. *Iso*-branching decreased the melting points of both CEs and WEs. In the case of CEs, *iso*-methyl branching caused a significant decrease in the melting point (from 90.3–91.4 °C to 66.5–67.1 °C) whereas the effect was less pronounced in the case of the WEs (from 47.0 –49.0 °C to 36.0 –37.5 °C). While the effect on the melting point is less pronounced in WEs, it can simultaneously be viewed as more important as branching brings it close to the ocular surface temperature. Altogether, the previous hypothesis seems valid although our results show that the decrease in melting point is highly dependent on the molecular structure and may differ substantially between distinct TFLL lipid classes. Nevertheless, since the CEs and WEs make up roughly 75–95% of meibum, the extensive chain branching observed in these species is probably essential in modulating the melting point and biophysical properties of meibum to a certain degree.

To investigate the effect of chain branching on the properties of CEs and WEs in more detail, WAXS studies were conducted on the synthesized lipids at room temperature and at physiological temperature. Through these studies, we expected to gain insights on the crystalline/amorphous nature of the lipid species and their packing/organization in the bulk state. This information could prove valuable in understanding their behavior in e.g. the crystalline structures formed by TFLL lipids [57,58].

The WAXS pattern of *n*-CE was similar to those displayed by shorter straight-chained CEs, such as cholesteryl myristate, cholesteryl palmitate, and cholesteryl stearate (Fig. 4) [59]. It was therefore possible to index the main peaks observed for *n*-CE using a monoclinic unit cell of $a = 10.23$ Å, $b = 7.6$ Å, $c = 131.5 \pm 0.3$ Å, $\beta = 94.4°$. The unit cell parameters reported for cholesteryl stearate were modified in order to correlate the *c* distance to the increased chain length [60]. The results matched those observed for saturated CEs in the bilayer crystal form [59], and thus, *n*-CE was interpreted to also crystallize in the bilayer form.

In contrast, the *iso*-CE showed a different WAXS pattern (Fig. 4), with a shorter long-spacing of 104.6 ± 1.0 Å, which does not correspond to any of the crystal forms reported previously for cholesteryl esters (bilayer, monolayer I, or monolayer II) (Supporting Fig. S26) [59]. While the observed long-spacing is shorter than those for the bilayer form, it is longer than those observed for the other crystal forms or the smectic liquid crystal phase, suggesting that *iso*-CE may crystallize as a perturbed bilayer to accommodate the methyl branch in the acyl chain. Further, the short spacing reflections differ from those observed for the bilayer crystal form, and *iso*-CE appears to be significantly more amorphous than *n*-CE, as indicated by the increased level of background, and also widths of the short spacing diffraction peaks, which indicate either smaller size and/or more disordered crystallites. This may be related to the fluidizing effect of the methyl branch, or possibly to other factors of unknown origin. Unfortunately, the amorphous nature of *iso*-CE did not allow a more detailed identification of its crystal form. Yet, it is clear that the *iso*-methyl branch inflicts a considerable change in the bulk structure and behavior of TFLL CEs.

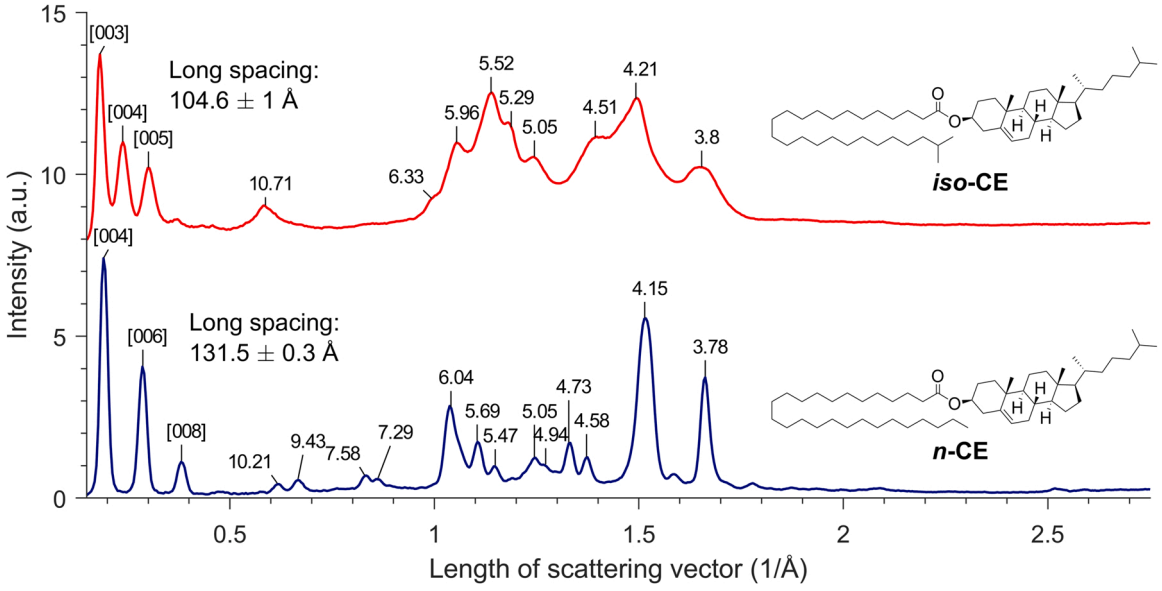

Fig. 4. WAXS patterns of *iso*-CE and *n*-CE at room temperature. Indexes of the long spacing peaks ([00 *l*]) are shown, along with the calculated long spacing values. For other peaks, the corresponding *d*-spacing values (Å) are shown.

n-WE and *iso*-WE also displayed a distinct difference in their WAXS patterns, which is indicative of deviating crystal forms (Fig. 5). For *n*-WE, the long spacing was determined to be 99.3 ± 0.4 Å based on multiple reflections, and the reflections corresponding to short spacings were observed at *d*-values of 4.13 Å, 4.25 Å, 4.34 Å, 3.7 Å, 3.83 Å, 4.53 Å, and 2.49 Å (in decreasing order of intensity). The prominent peaks at 4.13 Å and 3.7 Å would be characteristic of an orthorhombic structure in waxes [61–65]. However, due to the presence of the other strong reflections, the short-spacing reflections did not appear to directly correspond to any of the commonly observed methylene subcells [65]. Instead, they appear to be characteristic for wax esters containing a saturated alkoxy chain and an unsaturated acyl chain, since similar reflections were observed also for shorter wax esters such as: arachidyl oleate and behenyl oleate (Supporting Fig. S27) [66]. The long-spacings of this type of WEs were linearly dependent on the chain length, indicating that they crystallize in the same form (Supporting Fig. S28). Moreover, the lamellar spacings were similar to those previously reported for the orthorhombic β'-form of jojoba wax esters, suggesting that they may have some similarities [64].

The *iso*-WE on the other hand, displayed a WAXS pattern with a shorter long spacing (85.3 ± 0.2 Å). This long spacing value is significantly shorter than those reported for saturated wax esters and unsaturated jojoba wax esters (Supporting Fig. S28) [64,67,68], potentially suggesting a higher tilt in chain angle with respect to the lamellar interface. In contrast to *iso*-CE, *iso*-WE was only slightly more amorphous than *n*-WE, and a large number of reflections were observed in the short spacing region, with the most prominent peak found at *d*-value of 4.58 Å. This would typically correspond to a triclinic subcell but a detailed assignment was not possible based on the generated data alone. Nevertheless, the results confirm that the bulk crystal structure of branched TFLL WEs deviate from those of their straight-chain analogs, and, those reported earlier for other types of WEs.

While the *iso*-methyl branch altered the crystal form of both CEs and WEs at room temperature, we wanted to further investigate if there are significant differences in the crystal structures of these lipids at the physiological ocular surface temperature (34−35 °C) [69]. For *iso*-CE and *n*-CE, heating the samples to the ocular surface temperature had no effect on the WAXS patterns, likely due to their higher melting points. In contrast, heating *n*-WE to 34− 35 °C caused all the short spacing peaks to shift to larger *d*-spacing values by approximately 0.2 − 0.4%, while the long-spacing peaks were unaffected (Supporting Fig. S29). These subtle changes likely reflect the increased thermal motion in the crystal, which leads to an increase in the intermolecular distances, although the underlying lamellar organization is unaffected. An even larger expansion of the crystal structure appeared to occur in *iso*-WE, although quantitative analysis was not possible due to the partial melting of the sample at physiological temperature. Taken together, these result show that an *iso*-methyl branch has a considerable effect on the bulk properties and crystal structure of TFLL WEs and CEs. Moreover, the crystal structures of these species differ from those of many other known CEs and WEs. While these are important indications on their own, it should be noted that the bulk properties of TFLL CEs and WEs may not explain their biophysical profiles in the natural environment. In order to explore these, we next turned our attention to studying their biophysical properties at the aqueous interface, i.e. under conditions mimicking those at the ocular surface.

3.3. *Iso-methyl branching does not significantly affect the surface properties of CEs*

In order to uncover the surface properties displayed by the *iso*-methyl branched CEs and WEs (and compare these to the straight-chain analogs), and provide new insights on their potential roles in the TFLL, we devised a Langmuir trough based experimental study protocol. We have found the Langmuir trough to be an excellent model system for studying the properties of TFLL lipids under well-controlled conditions similar to those present at the ocular surface. In more detail, the aqueous subphase can be tailored to model the aqueous layer of the tear film, an eye blink can be simulated by compression/expansion cycles, the changes in biophysical properties of lipid films can be carefully analyzed by surface pressure/potential measurements, and Brewster angle microscopy (BAM) can be employed to monitor the visual changes occurring in the film. The only down side to this model system is that effects related to the flow of aqueous tears cannot be simulated, however, the advantages outweigh this minor disadvantage. In fact, when the advantages are further combined with access to synthetically pure TFLL lipids, a powerful tool for the comprehensive assessment of the biophysical profiles of TFLL lipids emerges.

The surface properties of straight-chain saturated and unsaturated cholesteryl esters have been studied previously by similar Langmuir monolayer techniques [6,9,16,70–76]. Based on the earlier studies, saturated CEs with more than 12 carbons in the acyl chain do not spread

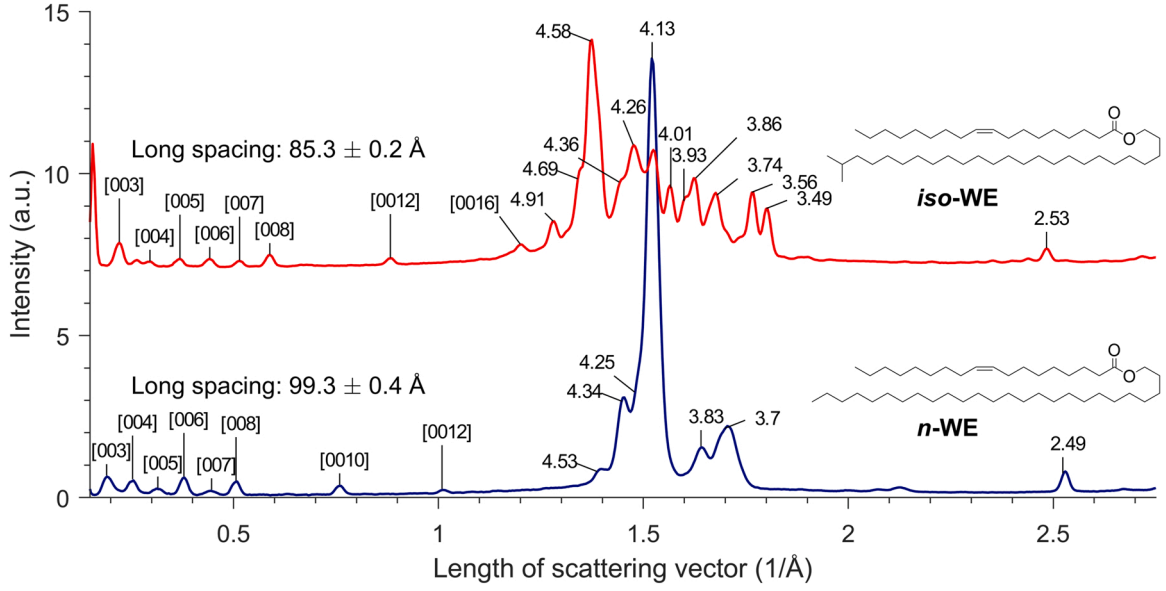

Fig. 5. WAXS patterns of *iso*-WE and *n*-WE at room temperature. Indexes of the long spacing peaks ([00 *l*]) are shown, along with the calculated long spacing values. For other peaks, the corresponding *d*-spacing values (Å) are shown.

at the aqueous surface. Instead they form crystalline domains, where the molecular orientation matches that of the bulk material [71–74,76]. On the other hand, unsaturated CEs have been shown to form multilamellar structures at the aqueous interface under suitable conditions [6,16,71,72].

In order to estimate the effect of *iso*-methyl branching on the interfacial organization of CEs, we first evaluated the behavior of *n*-CE at the water-air interface. While *n*-CE partially spread and formed a solid monolayer phase, the film also contained solid aggregates which were clearly seen as high intensity domains in the BAM-images (Fig. 6B,I). Upon compression, *n*-CE formed solid monolayer domains which were surrounded by solid aggregates (Fig. 6B,II). The surface pressure lift-off was 19 Å^2/molecule (Fig. 6A) which is reminiscent of a partial aggregation caused by the *n*-CE. Therefore, the results matched those obtained previously with shorter saturated straight-chained CEs. The *iso*-CE was found to behave in a similar manner (Fig. 6A & B,III–IV). Therefore, the differences noted for the bulk material in our preliminary WAXS studies did not manifest as different interfacial behavior. While subtle differences were noted in the surface potential isotherms of the two CEs studied (Supporting Fig. S30), the formation of aggregates limited the possibilities to draw definite conclusions based on these results. The lack of spreading capabilities at the aqueous interface likewise meant that neither *n*-CE, nor *iso*-CE, retarded evaporation of water (Fig. 6A) and thus their contribution to TFLL structure and function remains somewhat unclear. They may contribute to the overall organization of the TFLL, as noted in our recent studies [16], although more work is needed in order to fully understand the effects of the *iso*-methyl branch in such a scenario. Nevertheless, we do consider that the substantial decrease in the melting point caused by branching in CEs is likely essential to maintaining a sufficiently fluid meibum composition which can be secreted from the Meibomian glands to the ocular surface. Therefore, the extensive branching pattern observed in TFLL CEs may serve this particular purpose.

3.4. *Iso*-methyl branching promotes formation of solid WE monolayers with a moderate evaporation resistance

The formation of an evaporation resistance barrier is one of the key functions of the TFLL [77]. The evaporation resistance for the TFLL is often given using the s/cm scale. In order to consider the practicality of values on this scale, the model introduced by Cerretani et al. can be employed [19]. An evaporation resistance of 2 s/cm would reduce the evaporation rate at the ocular surface by 33–50%, while values such as 5 s/cm would correspond to a 60–80% reduction while a person is standing still or walking. The evaporation resistance of the TFLL is thought to be one of the essential mechanisms through which the tear film maintains the delicate balance between tear film renewal and its functional purpose. In fact, a dysfunctional TFLL is unable to efficiently uphold this regulatory function and the end result is an increased evaporation rate of aqueous tear fluid which leads to hyperosmolarity, which in turn is a condition closely associated with ocular surface diseases such as dry eye syndrome (DES) [78]. It has previously been suggested that WEs are important contributors to the TFLL evaporation resistance [11,14], and therefore studying the effect of the *iso*-methyl branch on their interfacial organization and evaporation resistance was warranted. In order for TFLL lipid species to be able to prevent the evaporation of aqueous tear fluid on a general level, they will need to be capable of forming a condensed phase with good coverage of the interfacial surface [66]. Otherwise, aqueous tear fluid may escape through "holes" in the monolayer or its boundaries. In practice, the central lipid species may form and sustain an evaporation resistant monolayer either through a transition from a liquid to a condensed phase [34], or, by direct spreading as a condensed monolayer phase [12]. These were the factors we sought to address in the present study.

We began by studying the *n*-WE using our Langmuir trough model system described above. Upon spreading, *n*-WE behaved similarly to the CEs. Initially, solid aggregates were formed (Fig. 7C,I), and when further compressed, a layer consisting of aggregates and partly spread wax ester was visible (Fig. 7C,II). This corresponds to the behavior reported previously for WEs with high melting points (melting points above the physiological one) [14]. Due to the lack of spreading and formation of a cohesive monolayer, *n*-WE was not capable of retarding the evaporation of water (Fig. 7B).

The melting point of *iso*-WE (36.0–37.5 °C) is close to the ocular surface temperature and thus a different biophysical profile was expected. In order to be thorough, the biophysical characterization of *iso*-WE was performed at temperatures both below (at 33 °C) and above (at 40 °C) its melting point. Upon spreading and compression at 40 °C, *iso*-WE formed a liquid monolayer (Fig. 7C,V), which collapsed at a low surface pressure (Fig. 7C,VI). The collapse was also seen as a plateau in the surface potential (Fig. 7A), which reached a constant value of approximately 250 mV. This value is in the same range as those previously reported for arachidyl oleate, behenyl oleate, and jojoba oil wax esters [21,79] and indicates a disordered monolayer structure, where

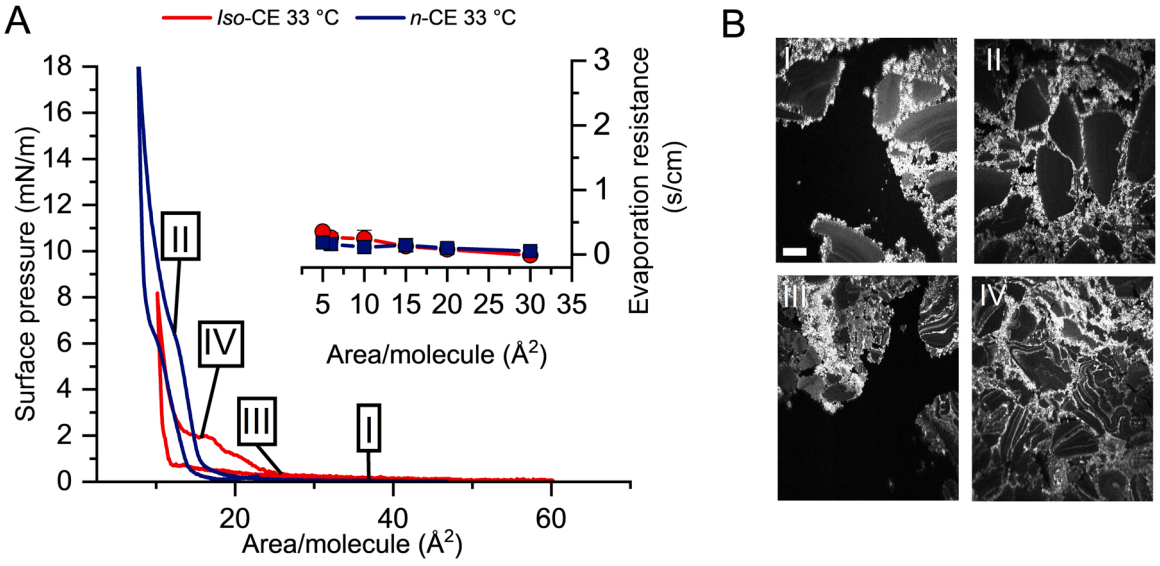

Fig. 6. (A) Representative surface pressure compression−expansion cycles of cholesteryl esters and their evaporation resistance (± SD, n = 3). (B) Corresponding Brewster angle microscopy images of cholesteryl ester films (I-II: *n*-CE, III-IV: *iso*-CE). The scale bar depicts 500 μm.

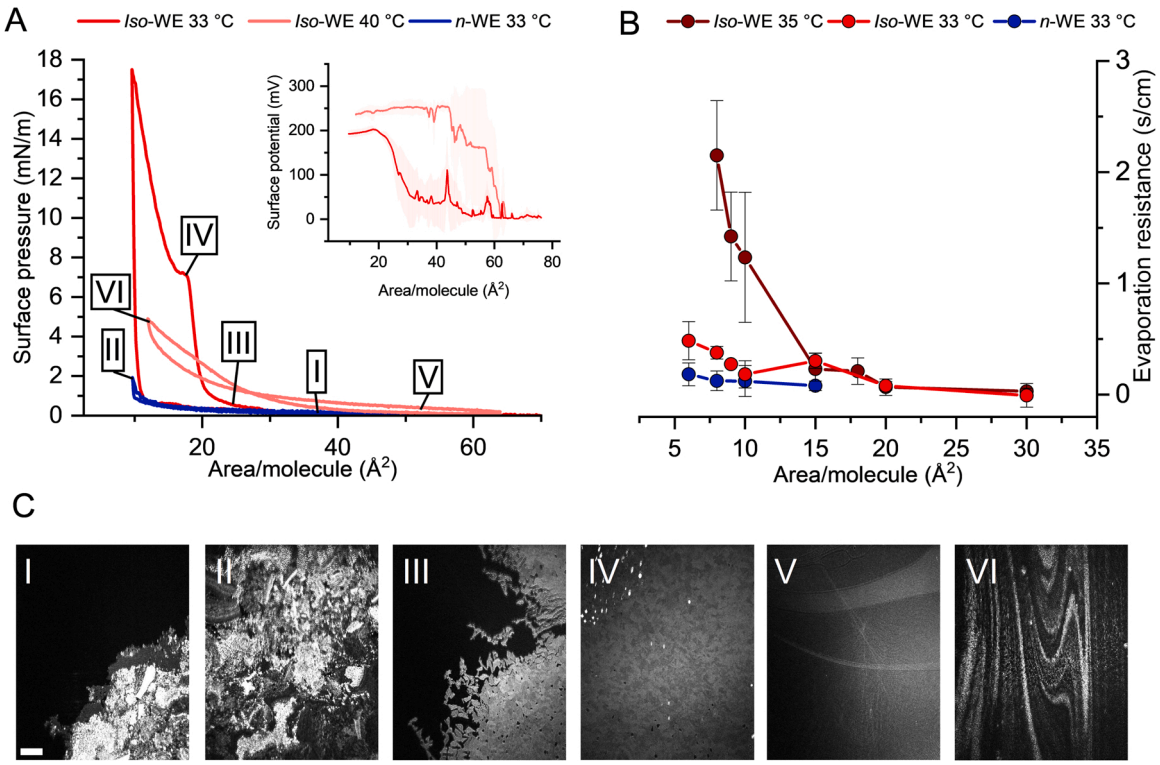

Fig. 7. (A) A representative surface-pressure compression−expansion cycle and the mean surface potential (± SD, n = 4) of WEs. (B) Evaporation resistance of wax esters as a function of mean molecular area (± SD, n = 4). (C) Corresponding BAM-pictures of WEs (I-II: *n*-WE 33 °C,III-IV: *iso*-WE 33 °C, V-VI: *iso*-WE 40 °C). The scale bar depicts 500 μm.

the ester groups are oriented towards the aqueous sub-phase. At physiological temperature, *iso*-WE formed solid monolayer islands with two different intensity levels as observed in the BAM-images (Fig. 7C, III). These findings suggest that regions with two distinct thicknesses were formed. When compressed, the islands merged to a uniform monolayer that covered the sub-phase surface (Fig. 7B, IV), and upon further compression, the film collapsed at 7.75 mN/m (Fig. 7A). These results indicated that the *iso*-methyl branch promoted spreading of *iso*-WE as a solid monolayer on the aqueous surface instead of the formation of aggregates. This also had a marked effect on its evaporation resistance properties which were found to be moderate (1.6−3.6 s/cm).

The difference observed between the organization and evaporation resistance of *iso*-WE and *n*-WE are likely connected to their melting points. In more detail, Rantamäki et al. have shown that WEs retard evaporation at temperatures near their melting point [12]. Apparently, this also applies to *iso*-branched WEs. In other words, the monolayer structure formed by *iso*-WE was sufficiently condensed to promote evaporation resistance at the physiological temperature. However, the evaporation resistance observed for pure *iso*-WE was modest, especially when compared to our recent results on mixtures of OAHFAs and WEs [66]. This suggests that the cooperative interactions between different TFLL lipid classes may be a key factor in reaching the reported TFLL evaporation resistance (9 s/cm) [80,81]. Nevertheless, based on the differences observed in straight- and branched WEs herein, it is clear that branching alters the biophysical properties of these species and consequently affects the structure and function of the TFLL on the whole. Therefore, in future studies on TFLL WEs, it is highly recommended to take into account the extensive branching patterns as the results obtained with simplified analogs may no longer be representative of the majority of the TFLL WEs [1].

4. Conclusions

During the past years, we have focused our efforts on generating an increased understanding of the structure and function of the TFLL through a bottom-up approach involving the synthesis and biophysical characterization of the major lipid classes present therein. Herein, we continued these studies by a detailed assessment of the properties of *iso*-methyl branched WEs and CEs, and their straight-chain analogs, since these together make up the majority of the TFLL lipidome. We described the total synthesis and complete NMR-spectroscopic characterization of the major lipid species belonging to the WE and CE categories, i.e. *iso*-WE (**4**) and *iso*-CE (**6**) (and the corresponding *n*-WE and *n*-CE). In addition, we performed a detailed characterization on the effects caused by the *iso*-branch on the biophysical profiles of TFLL lipids (e.g., the melting points, crystal structures, interfacial organization, and evaporation resistance). We found that the *iso*-methyl branch inflicts a significant change in the biophysical properties of TFLL lipids on multiple levels which are not possible to emulate with straight-chain model compounds alone. Our results prove that these factors need to be accounted for in future studies in order to correctly convey the properties of the naturally occurring TFLL WEs and CEs.

CRediT authorship contribution statement

Tuomo Viitaja: Conceptualization, Investigation, Methodology, Formal Analysis, Writing, Funding Acquisition. **Jan-Erik:** Raitanen: Conceptualization, Investigation, Methodology, Writing. **Antti Hynynen:** Investigation, Validation. **Jukka Moilanen:** Conceptualization, Supervision, Resources, Funding acquisition. **Kirsi Svedström:** Conceptualization, Investigation, Methodology, Resources, Writing, Funding acquisition. **Riku O. Paananen:** Conceptualization, Investigation, Writing, Funding acquisition, Project administration. **Filip S. Ekholm:** Conceptualization, Investigation, Methodology, Writing, Supervision, Funding acquisition, Project administration.

Declaration of Competing Interest

The authors declare that they have no known competing financial interests or personal relationships that could have appeared to influence the work reported in this paper.

Acknowledgements

Financial support from the Eye and Tissue Bank Foundation, the Mary and Georg C. Ehrnrooth Foundation, the Ruth and Nils-Erik Stenbäck Foundation, the Vilho, Yrjö, and Kalle Väisälä Foundation, the Swedish Cultural Foundation, the Evald and Hilda Nissi Foundation, the Academy of Finland, Business Finland, and the Finnish Eye Foundation is gratefully acknowledged. The authors further thank BSc. student Cordula Schlegel (University of Helsinki) for laboratory assistance and the staff at the workshop of the Faculty of Science, University of Helsinki for access to custom made materials and equipment.

Appendix A. Supporting information

Supplementary data associated with this article can be found in the online version at doi:10.1016/j.colsurfb.2022.112429.

References

[1] N. Nicolaides, J.K. Kaitaranta, T.N. Rawdah, J.I. Macy, F.M. Boswell 3rd, R. E. Smith, Meibomian gland studies: comparison of steer and human lipids, Invest. Ophthalmol. Vis. Sci. 20 (4) (1981) 522–536.
[2] J. Chen, K.B. Green, K.K. Nichols, Quantitative profiling of major neutral lipid classes in human meibum by direct infusion electrospray ionization mass spectrometry, Invest. Ophthalmol. Vis. Sci. 54 (8) (2013) 5730, https://doi.org/10.1167/iovs.12-10317.
[3] I.A. Butovich, Tear film lipids, Exp. Eye Res. 117 (2013) 4–27, https://doi.org/10.1016/j.exer.2013.05.010.
[4] S.H.J. Brown, C.M.E. Kunnen, E. Duchoslav, N.K. Dolla, M.J. Kelso, E.B. Papas, P. Lazon de la Jara, M.D.P. Willcox, S.J. Blanksby, T.W. Mitchell, A Comparison of patient matched meibum and tear lipidomes, Invest. Ophthalmol. Vis. Sci. 54 (12) (2013) 7417, https://doi.org/10.1167/iovs.13-12916.
[5] S.M. Lam, L. Tong, B. Reux, X. Duan, A. Petznick, S.S. Yong, C.B.S. Khee, M.J. Lear, M.R. Wenk, G. Shui, Lipidomic analysis of human tear fluid reveals structure-specific lipid alterations in dry eye syndrome, J. Lipid Res. 55 (2) (2014) 299–306, https://doi.org/10.1194/jlr.P041780.
[6] T.J. Millar, P.E. King-Smith, Analysis of comparison of human meibomian lipid films and mixtures with cholesteryl esters in vitro films using high resolution color microscopy, Invest. Ophthalmol. Vis. Sci. 53 (8) (2012) 4710, https://doi.org/10.1167/iovs.12-10022.
[7] B.S. Schuett, T.J. Millar, Lipid component contributions to the surface activity of meibomian lipids, Invest. Ophthalmol. Vis. Sci. 53 (11) (2012) 7208, https://doi.org/10.1167/iovs.12-10471.
[8] B.S. Schuett, T.J. Millar, An investigation of the likely role of (O-acyl) ω-hydroxy fatty acids in meibomian lipid films using (O-oleyl) ω-hydroxy palmitic acid as a model, Exp. Eye Res. 115 (2013) 57–64, https://doi.org/10.1016/j.exer.2013.06.016.
[9] P. Kulovesi, J. Telenius, A. Koivuniemi, G. Brezesinski, I. Vattulainen, J. M. Holopainen, The impact of lipid composition on the stability of the tear fluid lipid layer, Soft Matter 8 (21) (2012) 5826, https://doi.org/10.1039/c2sm25210d.
[10] P. Kulovesi, J. Telenius, A. Koivuniemi, G. Brezesinski, A. Rantamäki, T. Viitala, E. Puukilainen, M. Ritala, S.K. Wiedmer, I. Vattulainen, J.M. Holopainen, Molecular organization of the tear fluid lipid layer, Biophys. J. 99 (8) (2010) 2559–2567, https://doi.org/10.1016/j.bpj.2010.08.001.
[11] A.H. Rantamäki, M. Javanainen, I. Vattulainen, J.M. Holopainen, Do lipids retard the evaporation of the tear fluid? Invest. Ophthalmol. Vis. Sci. 53 (10) (2012) 6442, https://doi.org/10.1167/iovs.12-10487.
[12] A.H. Rantamäki, S.K. Wiedmer, J.M. Holopainen, Melting points—the key to the anti-evaporative effect of the tear film wax esters, Invest. Ophthalmol. Vis. Sci. 54 (8) (2013) 5211, https://doi.org/10.1167/iovs.13-12408.
[13] P. Kulovesi, A.H. Rantamäki, J.M. Holopainen, Surface properties of artificial tear film lipid layers: effects of wax esters, Invest. Ophthalmol. Vis. Sci. 55 (7) (2014) 4448, https://doi.org/10.1167/iovs.14-14122.
[14] R.O. Paananen, A.H. Rantamäki, J.M. Holopainen, Antievaporative mechanism of wax esters: implications for the function of tear fluid, Langmuir 30 (20) (2014) 5897–5902, https://doi.org/10.1021/la501678t.
[15] A.H. Rantamäki, J.M. Holopainen, The effect of phospholipids on tear film lipid layer surface activity, Invest. Ophthalmol. Vis. Sci. 58 (1) (2017) 149, https://doi.org/10.1167/iovs.16-20468.
[16] R.O. Paananen, T. Viitaja, A. Olżyńska, F.S. Ekholm, J. Moilanen, L. Cwiklik, Interactions of polar lipids with cholesteryl ester multilayers elucidate tear film lipid layer structure, Ocul. Surf. 18 (4) (2020) 545–553, https://doi.org/10.1016/j.jtos.2020.06.001.
[17] Z.A. Hetman, D. Borchman, Concentration dependent cholesteryl-ester and wax-ester structural relationships and meibomian gland dysfunction, Biochem. Biophys. Rep. 21 (2020), 100732, https://doi.org/10.1016/j.bbrep.2020.100732.
[18] P.G. Petrov, J.M. Thompson, I.B.A. Rahman, R.E. Ellis, E.M. Green, F. Miano, C. P. Winlove, Two-dimensional order in mammalian pre-ocular tear film, Exp. Eye Res. 84 (6) (2007) 1140–1146, https://doi.org/10.1016/j.exer.2007.02.012.
[19] C.F. Cerretani, N.H. Ho, C.J. Radke, Water-evaporation reduction by duplex films: application to the human tear film, Adv. Colloid Interface Sci. 197–198 (2013) 33–57, https://doi.org/10.1016/j.cis.2013.03.007.
[20] T.F. Svitova, M.C. Lin, Evaporation retardation by model tear-lipid films: the roles of film aging, compositions and interfacial rheological properties, Colloids Surf. B 197 (2021), 111392, https://doi.org/10.1016/j.colsurfb.2020.111392.
[21] R.O. Paananen, M. Javanainen, J.M. Holopainen, I. Vattulainen, Crystalline wax esters regulate the evaporation resistance of tear film lipid layers associated with dry eye syndrome, J. Phys. Chem. Lett. 10 (14) (2019) 3893–3898, https://doi.org/10.1021/acs.jpclett.9b01187.
[22] J.S. Andrews, Human tear film lipids, Exp. Eye Res. 10 (2) (1970) 223–227, https://doi.org/10.1016/S0014-4835(70)80032-X.
[23] J.M. Tiffany, The lipid secretion of the meibomian glands, Adv. Lipid Res. (1987) 1–62, https://doi.org/10.1016/B978-0-12-024922-0.50005-9.
[24] D. Borchman, A. Ramasubramanian, Human meibum chain branching variability with age, gender and meibomian gland dysfunction, Ocul. Surf. 17 (2) (2019) 327–335, https://doi.org/10.1016/j.jtos.2018.12.005.
[25] I.A. Butovich, A. McMahon, J.C. Wojtowicz, F. Lin, R. Mancini, K. Itani, Dissecting lipid metabolism in meibomian glands of humans and mice: an integrative study reveals a network of metabolic reactions not duplicated in other tissues, Biochim. Biophys. Acta 1861 (6) (2016) 538–553, https://doi.org/10.1016/j.bbalip.2016.03.024.
[26] J. Cason, Branched-chain fatty acids. VI. relationship of melting point to structure. New method of synthesis of acids containing a quaternary carbon atom, J. Org. Chem. 13 (2) (1948) 227–238, https://doi.org/10.1021/jo01160a010.
[27] F.M. Menger, M.G. Wood, Q.Z. Zhou, H.P. Hopkins, J. Fumero, Thermotropic properties of synthetic chain-substituted phosphatidylcholines: effect of substituent size, polarity, number, and location on molecular packing in bilayers, J. Am. Chem. Soc. 110 (20) (1988) 6804–6810, https://doi.org/10.1021/ja00228a033.
[28] D. Poger, B. Caron, A.E. Mark, Effect of methyl-branched fatty acids on the structure of lipid bilayers, J. Phys. Chem. B 118 (48) (2014) 13838–13848, https://doi.org/10.1021/jp503910r.
[29] A.W. Weitkamp, The acidic constituents of degras. a new method of structure elucidation [1], J. Am. Chem. Soc. 67 (3) (1945) 447–454, https://doi.org/10.1021/ja01219a027.
[30] J.R. Silvius, R.N. McElhaney, Effects of phospholipid acyl chain structure on physical properties: I. Isobranched phosphatidylcholines, Chem. Phys. Lipids 24 (3) (1979) 287–296, https://doi.org/10.1016/0009-3084(79)90034-3.
[31] R. Laatikainen, M. Niemitz, U. Weber, J. Sundelin, T. Hassinen, J. Vepsäläinen, General strategies for total-lineshape-type spectral analysis of nmr spectra using integral-transform iterator, J. Magn. Reson, Ser. A 120 (1) (1996) 1–10, https://doi.org/10.1006/jmra.1996.0094.
[32] R.O. Paananen, A.H. Rantamäki, J. Parshintsev, J.M. Holopainen, The effect of ambient ozone on unsaturated tear film wax esters, Invest. Ophthalmol. Vis. Sci. 56 (13) (2015) 8054, https://doi.org/10.1167/iovs.15-18398.
[33] I. Langmuir, V.J. Schaefer, Rates of evaporation of water through compressed monolayers on water, J. Frankl. Inst. 235 (2) (1943) 119–162, https://doi.org/10.1016/S0016-0032(43)90904-4.
[34] H.C. Bland, J.A. Moilanen, F.S. Ekholm, R.O. Paananen, Investigating the role of specific tear film lipids connected to dry eye syndrome: a study on *O* -Acyl-ω-Hydroxy fatty acids and diesters, Langmuir 35 (9) (2019) 3545–3552, https://doi.org/10.1021/acs.langmuir.8b04182.
[35] T. Viitaja, J.-E. Raitanen, J. Moilanen, R.O. Paananen, F.S. Ekholm, The properties and role of *O*-Acyl-ω-Hydroxy fatty acids and type I-St and type II diesters in the tear film lipid layer revealed by a combined chemistry and biophysics approach, J. Org. Chem. 86 (7) (2021) 4965–4976, https://doi.org/10.1021/acs.joc.0c02882.
[36] S.M. Lam, L. Tong, S.S. Yong, B. Li, S.S. Chaurasia, G. Shui, M.R. Wenk, Meibum lipid composition in asians with dry eye disease, PLoS One 6 (10) (2011), e24339, https://doi.org/10.1371/journal.pone.0024339.
[37] J. Chen, K.B. Green-Church, K.K. Nichols, Shotgun lipidomic analysis of human meibomian gland secretions with electrospray ionization tandem mass spectrometry, Invest. Ophthalmol. Vis. Sci. 51 (12) (2010) 6220, https://doi.org/10.1167/iovs.10-5687.
[38] I.A. Butovich, E. Uchiyama, J.P. McCulley, Lipids of human meibum: mass-spectrometric analysis and structural elucidation, J. Lipid Res. 48 (10) (2007) 2220–2235, https://doi.org/10.1194/jlr.M700237-JLR200.
[39] S.E. Hancock, R. Ailuri, D.L. Marshall, S.H.J. Brown, J.T. Saville, V.R. Narreddula, N.R. Boase, B.L.J. Poad, A.J. Trevitt, M.D.P. Willcox, M.J. Kelso, T.W. Mitchell, S. J. Blanksby, Mass spectrometry-directed structure elucidation and total synthesis of ultra-long chain (*O* -Acyl)-ω-Hydroxy fatty acids, J. Lipid Res. 59 (8) (2018) 1510–1518, https://doi.org/10.1194/jlr.M086702.
[40] L. Balas, J. Bertrand-Michel, F. Viars, J. Faugere, C. Lefort, S. Caspar-Bauguil, D. Langin, T. Durand, Regiocontrolled syntheses of FAHFAs and LC-MS/MS differentiation of regioisomers, Org. Biomol. Chem. 14 (38) (2016) 9012–9020, https://doi.org/10.1039/C6OB01597B.
[41] L.A. Robertson, D.L. Gin, Effect of an *n* -Alkoxy-2,4-Hexadiene polymerizable tail system on the mesogenic properties and cross-linking of mono-imidazolium-based

ionic liquid crystal monomers, ACS Macro Lett. 5 (7) (2016) 844–848, https://doi.org/10.1021/acsmacrolett.6b00315.
[42] S. Chanda, S. Ramakrishnan, Poly(Alkylene Itaconate)s – an interesting class of polyesters with periodically located exo-chain double bonds susceptible to michael addition, Polym. Chem. 6 (11) (2015) 2108–2114, https://doi.org/10.1039/C4PY01613K.
[43] J. Greaves, K.R. Munro, S.C. Davidson, M. Riviere, J. Wojno, T.K. Smith, N.C. O. Tomkinson, L.H. Chamberlain, Molecular basis of fatty acid selectivity in the ZDHHC family of s-acyltransferases revealed by click chemistry, Proc. Natl. Acad. Sci. USA 114 (8) (2017) E1365–E1374, https://doi.org/10.1073/pnas.1612254114.
[44] M.C. Wamberg, R. Wieczorek, S.B. Brier, J.W. de Vries, M. Kwak, A. Herrmann, P.-A. Monnard, Functionalization of fatty acid vesicles through newly synthesized bolaamphiphile–DNA conjugates, Bioconjug. Chem. 25 (9) (2014) 1678–1688, https://doi.org/10.1021/bc500289u.
[45] A. Beck, D. Heissler, G. Duportail, Synthesis of fluorescent probes for localized membrane fluidity measurements, Tetrahedron 47 (8) (1991) 1459–1472, https://doi.org/10.1016/S0040-4020(01)86422-X.
[46] A. Sharma, I. Ramos-Tomillero, A. El-Faham, E. Nicolas, H. Rodriguez, B. G. delaTorre, F. Albericio, Understanding tetrahydropyranyl as a protecting group in peptide chemistry, ChemistryOpen 6 (2) (2017) 168–177, https://doi.org/10.1002/open.201600156.
[47] S. Nayak, B. Sahoo, T.K. Chaki, D. Khastgir, Facile preparation of uniform barium titanate ($BaTiO_3$) multipods with high permittivity: impedance and temperature dependent dielectric behavior, RSC Adv. 4 (3) (2014) 1212–1224, https://doi.org/10.1039/C3RA44815K.
[48] M.U. Roslund, P. Tähtinen, M. Niemitz, R. Sjöholm, Complete assignments of the 1H and 13C chemical shifts and JH,H coupling constants in NMR spectra of d-Glucopyranose and All d-Glucopyranosyl-d-Glucopyranosides, Carbohydr. Res. 343 (1) (2008) 101–112, https://doi.org/10.1016/j.carres.2007.10.008.
[49] F.S. Ekholm, A. Ardá, P. Eklund, S. André, H.-J. Gabius, J. Jiménez-Barbero, R. Leino, Studies related to norway spruce galactoglucomannans: chemical synthesis, conformation analysis, nmr spectroscopic characterization, and molecular recognition of model compounds, Chem. Eur. J. 18 (45) (2012) 14392–14405, https://doi.org/10.1002/chem.201200510.
[50] D. Díaz, A. Canales-Mayordomo, F.J. Cañada, J. Jiménez-Barbero, Solution conformation of carbohydrates: a view by using nmr assisted by modeling, Methods Mol. Biol. 1273 (2015) 261–287, https://doi.org/10.1007/978-1-4939-2343-4_19.
[51] I.A. Butovich, J.C. Wojtowicz, M. Molai, Human tear film and meibum. very long chain wax esters and (O-Acyl)-Omega-Hydroxy fatty acids of meibum, J. Lipid Res. 50 (12) (2009) 2471–2485, https://doi.org/10.1194/jlr.M900252-JLR200.
[52] I.A. Butovich, On the presence of (O-Acyl)-Omega-Hydroxy fatty acids and of their esters in human meibomian gland secretions, Invest. Ophthalmol. Vis. Sci. 52 (1) (2011) 639, https://doi.org/10.1167/iovs.10-7028.
[53] D.J. Frost, F.D. Gunstone, The PMR analysis of non-conjugated alkenoic and alkynoic acids and esters, Chem. Phys. Lipids 15 (1) (1975) 53–85, https://doi.org/10.1016/0009-3084(75)90032-8.
[54] T.K. Kotammagari, S. Paul, A.K. Bhattacharya, Unusual epimerization in styryllactones: synthesis of (−)-5-Hydroxygoniothalamin, (−)-5-Acetylgoniothalamin, and *O* -TBS-Goniopypyrone, ACS Omega 4 (27) (2019) 22549–22556, https://doi.org/10.1021/acsomega.9b03263.
[55] B. Pérez, S.E. Dahlgaard, P. Bulsara, A.V. Rawlings, M.M. Jensen, M. Dong, M. Glasius, M.J. Clarke, Z. Guo, Synthesis and characterization of O-Acylated-ω-Hydroxy fatty acids as skin-protecting barrier lipids, J. Colloid Interface Sci. 490 (2017) 137–146, https://doi.org/10.1016/j.jcis.2016.11.031.
[56] A.H. Milburn, E.V. Truter, The components of wool wax. Part II. synthesis of the acids and alcohols of the Iso- and the (+)-Anteiso-series, J. Chem. Soc. (1954) 3344, https://doi.org/10.1039/jr9540003344.
[57] D.L. Leiske, C.E. Miller, L. Rosenfeld, C. Cerretani, A. Ayzner, B. Lin, M. Meron, M. Senchyna, H.A. Ketelson, D. Meadows, S. Srinivasan, L. Jones, C.J. Radke, M. F. Toney, G.G. Fuller, Molecular structure of interfacial human meibum films, Langmuir 28 (32) (2012) 11858–11865, https://doi.org/10.1021/la301321r.
[58] L. Rosenfeld, C. Cerretani, D.L. Leiske, M.F. Toney, C.J. Radke, G.G. Fuller, Structural and rheological properties of meibomian lipid, Invest. Ophthalmol. Vis. Sci. 54 (4) (2013) 2720, https://doi.org/10.1167/iovs.12-10987.
[59] G.S. Ginsburg, D. Atkinson, D.M. Small, Physical properties of cholesteryl esters, Prog. Lipid Res. 23 (3) (1984) 135–167, https://doi.org/10.1016/0163-7827(84)90002-X.
[60] J.H. Wendorff, F.P. Price, An X-Ray diffraction study of crystalline cholesteryl myristate and cholesteryl stearate, Mol. Cryst. Liq. 22 (1–2) (1973) 85–97, https://doi.org/10.1080/15421407308083336.
[61] R.D. Heyding, K.E. Russell, T.L. Varty, D. St-Cyr, The normal paraffins revisited, Powder Diffr. 5 (2) (1990) 93–100, https://doi.org/10.1017/S0885715600015414.
[62] H.J. Ensikat, M. Boese, W. Mader, W. Barthlott, K. Koch, Crystallinity of plant epicuticular waxes: electron and X-Ray diffraction studies, Chem. Phys. Lipids 144 (1) (2006) 45–59, https://doi.org/10.1016/j.chemphyslip.2006.06.016.
[63] F.R.L. Schoening, The X-Ray diffraction pattern and deformation texture of beeswax, S. Afr. J. Sci. 76 (6) (1980) 262–265.
[64] L. Bouzidi, S. Li, S. Di Biase, S.Q. Rizvi, S.S. Narine, Lubricating and waxy esters, I. synthesis, crystallization, and melt behavior of linear monoesters, Chem. Phys. Lipids 165 (1) (2012) 38–50, https://doi.org/10.1016/j.chemphyslip.2011.11.003.
[65] D.L. Dorset, Crystallography of the Polymethylene Chain, Oxford University Press, 2004, https://doi.org/10.1093/acprof:oso/9780198529088.001.0001.
[66] T. Viitaja, J. Moilanen, K.J. Svedström, F.S. Ekholm, R.O. Paananen, Tear film lipid layer structure: self-assembly of *O*-Acyl-ω-Hydroxy fatty acids and wax esters into evaporation-resistant monolayers, Nano Lett. 21 (18) (2021) 7676–7683, https://doi.org/10.1021/acs.nanolett.1c02475.
[67] S. Aleby, I. Fischmeister, B.T.R. Iyengar, The infrared spectra and polymorphism of long chain esters: IV. some esters from tetradecanol, hexadecanol, octadecanol, eicosanol, docosanol and dodecanoic, tetradecanoic, hexadecanoic, octadecanoic and eicosanoic acid, Lipids 6 (6) (1971) 421–425, https://doi.org/10.1007/BF02531380.
[68] D.A. Lutz, C.R. Eddy, J.J. Hunter, X-Ray diffraction study of some normal alkyl esters of long-chain acids, Lipids 2 (3) (1967) 204–207, https://doi.org/10.1007/BF02532556.
[69] C. Purslow, J.S. Wolffsohn, Ocular surface temperature: a review, Eye Contact Lens 31 (3) (2005) 117–123, https://doi.org/10.1097/01.ICL.0000141921.80061.17.
[70] P. Xavier, S. Brindhu Malani, P. Viswanath, The role of molecular packing in dictating the miscibility of some cholesteryl *n* -Alkanoates at interfaces, Langmuir 37 (38) (2021) 11203–11211, https://doi.org/10.1021/acs.langmuir.1c01025.
[71] J.M. Smaby, H.L. Brockman, Novel surface phase containing cholesteryl esters. 1. structural characteristics determined from surface pressure-area measurements, Biochemistry 20 (4) (1981) 718–723, https://doi.org/10.1021/bi00507a008.
[72] J.M. Smaby, H.L. Brockman, Novel surface phase containing cholesteryl esters. 2. nonequivalence of cholesteryl arachidonate and those with 18-carbon, cis-unsaturated acyl groups, Biochemistry 20 (4) (1981) 724–730, https://doi.org/10.1021/bi00507a009.
[73] J.M. Smaby, W.J. Baumann, H.L. Brockman, Lipid structure and the behavior of cholesteryl esters in monolayer and bulk phases, J. Lipid Res. 20 (6) (1979) 789–795, https://doi.org/10.1016/S0022-2275(20)40032-X.
[74] P. Viswanath, K.A. Suresh, Monolayers and 3D films of cholesteryl derivatives at the air−water interface, J. Phys. Chem. B 108 (26) (2004) 9198–9207, https://doi.org/10.1021/jp049454z.
[75] C. Alonso, I. Kuzmenko, T.R. Jensen, K. Kjaer, M. Lahav, L. Leiserowitz, Self-assembly of crystalline films of interdigitated long-chain cholesteryl esters at the air−water interface, J. Phys. Chem. B 105 (36) (2001) 8563–8568, https://doi.org/10.1021/jp010658e.
[76] A. Sarkar, K.A. Suresh, Self-assembly and molecular packing in cholesteryl esters at interfaces, J. Chem. Phys. 146 (21) (2017), 214702, https://doi.org/10.1063/1.4984119.
[77] P.E. King-Smith, M.D. Bailey, R.J. Braun, Four characteristics and a model of an effective tear film lipid layer (TFLL), Ocul. Surf. 11 (4) (2013) 236–245, https://doi.org/10.1016/j.jtos.2013.05.003.
[78] A.J. Bron, C.S. de Paiva, S.K. Chauhan, S. Bonini, E.E. Gabison, S. Jain, E. Knop, M. Markoulli, Y. Ogawa, V. Perez, Y. Uchino, N. Yokoi, D. Zoukhri, D.A. Sullivan, TFOS DEWS II pathophysiology report, Ocul. Surf. 15 (3) (2017) 438–510, https://doi.org/10.1016/j.jtos.2017.05.011.
[79] B. Caruso, M.F. Martini, M. Pickholz, M.A. Perillo, V-Shaped molecular configuration of wax esters of jojoba oil in a langmuir film model, Langmuir 34 (26) (2018) 7887–7898, https://doi.org/10.1021/acs.langmuir.8b00693.
[80] S. Iwata, M.A. Lemp, F.J. Holly, C.H. Dohlman, Evaporation rate of water from the precorneal tear film and cornea in the rabbit, Invest. Ophthalmol. Vis. Sci. 8 (6) (1969) 613–619.
[81] C.-C. Peng, C. Cerretani, Y. Li, S. Bowers, S. Shahsavarani, M.C. Lin, C.J. Radke, Flow evaporimeter to assess evaporative resistance of human tear-film lipid layer, Ind. Eng. Chem. Res. 53 (47) (2014) 18130–18139, https://doi.org/10.1021/ie5030497.